

# Why the Lysogenic State of Phage $\lambda$ Is So Stable: A Mathematical Modeling Approach

Moisés Santillán\* and Michael C. Mackey†

\*Centre for Nonlinear Dynamics, McGill University, H3G 1Y6 Montreal, Quebec, Canada; and †Departments of Physiology, Physics & Mathematics and Centre for Nonlinear Dynamics, McGill University, H3G 1Y6 Montreal, Quebec, Canada

**ABSTRACT** We develop a mathematical model of the phage  $\lambda$  lysis/lysogeny switch, taking into account recent experimental evidence demonstrating enhanced cooperativity between the left and right operator regions. Model parameters are estimated from available experimental data. The model is shown to have a single stable steady state for these estimated parameter values, and this steady state corresponds to the lysogenic state. When the CI degradation rate ( $\gamma_{ci}$ ) is slightly increased from its normal value ( $\gamma_{ci} \simeq 0.0 \text{ min}^{-1}$ ), two additional steady states appear (through a saddle-node bifurcation) in addition to the lysogenic state. One of these new steady states is stable and corresponds to the lytic state. The other steady state is an (unstable) saddle node. The coexistence these two globally stable steady states (the lytic and lysogenic states) is maintained with further increases of  $\gamma_{ci}$  until  $\gamma_{ci} \simeq 0.35 \text{ min}^{-1}$ , when the lysogenic steady state and the saddle node collide and vanish (through a reverse saddle node bifurcation) leaving only the lytic state surviving. These results allow us to understand the high degree of stability of the lysogenic state because, normally, it is the only steady state. Further implications of these results for the stability of the phage  $\lambda$  switch are discussed, as well as possible experimental tests of the model.

## INTRODUCTION

Bacteriophage (or simply phage)  $\lambda$  is a virus capable of infecting *Escherichia coli* bacteria. After infection, the virus can follow either one of two different pathways: 1), the virus integrates its DNA into the host bacterial DNA and duplicates when the bacterium divides (this pathway is known as lysogeny); 2), the virus uses the bacterial molecular machinery to make many viral copies and leave (after killing the host bacterium) to infect other bacteria (the so-called lysis pathway). Once the virus is in the lysogenic state, it can shift to the lysis state under certain conditions, e.g., if the bacterial culture is irradiated with ultraviolet (UV) light. The molecular regulatory mechanism responsible for the lysogeny/lysis decision is known as the phage  $\lambda$  switch.

The two patterns of phage  $\lambda$  behavior, lytic and lysogenic, and the subtle ways in which it subverts its host, *E. coli*, have made it a paradigm for many biological pathways (Gottesman, 1999). One of the most striking characteristics of the phage  $\lambda$  switch is the fact that the intrinsic loss rate of  $\lambda$  lysogeny is of the order of  $10^{-7}$  per cell and generation (Aurell et al., 2002; Little et al., 1999; Rozanov et al., 1998). In contrast, the mutation rate in the portion of the  $\lambda$  genome involved in lysogeny is between  $10^{-6}$  and  $10^{-7}$  per generation (Aurell et al., 2002; Little et al., 1999). Thus, the lysogenic state is more stable than the genome itself.

The large volume of experimental data on the behavior of this system and the logical structure underlying the switch

performance make it appealing for mathematical modeling. Several mathematical models have been proposed in the last two decades to explain the astonishingly high degree of stability of the phage  $\lambda$  lysogenic state. Nevertheless, to our knowledge, both the stability of the lysogenic state and the efficiency of the switch still lack a proper explanation. The aim of this paper is to offer an explanation of the lysogenic state stability based on a new modeling effort. Below, we briefly review some of the existing models of the phage  $\lambda$  switch before turning to an exposition of our results.

The first model incorporating quantitative biochemical information was proposed by Ackers et al. (1982). This is an equilibrium model that explains the existence of the lytic and lysogenic steady states, but not their relative stability. Later, Shea and Ackers (1985) improved their model making it fully dynamical. This model gave the expected qualitative behavior for stable maintenance of lysogeny, as well as for the induction of lysis. Reinitz and Vaisnys (1990) extended the dynamical model, and found a quantitative inconsistency between their experiments and the model predictions. The most extensive model was developed by McAdams and Shapiro (1995) who included all of the proteins involved in the lysis/lysogeny switch, as well as the genes that become active after the fate of the phage is determined. Arkin et al. (1998) published a model of the  $\lambda$  switch based on a stochastic representation of transcription, translation, and interaction between proteins. They accurately predicted the fraction of lysogens developed after infection. Further, their simulations clearly show how two identical cells in identical conditions, infected with the same number of phage, can still meet different fates. More recently, Aurell and Sneppen (2002) and Aurell et al. (2002) studied the stability of the lysogenic state using a stochastic mathematical model. From their results, they suggested that the current view of the phage  $\lambda$  switch is incomplete, given the difference they

Submitted May 12, 2003, and accepted for publication September 16, 2003.

Address reprint requests to Moisés Santillán, Depto. de Física, Esc. Sup. de Física y Matemáticas, Inst. Politécnico Nal. 07738 México D.F., México. Tel.: +52-55-57296000 ext. 55319; Fax: +52-55-57296000 ext. 55051; E-mail: moyo@esfm.ipn.mx.

Moisés Santillán is currently an invited researcher at Departamento de Matemáticas, Centro de Investigación y Estudios Avanzados del IPN.

© 2004 by the Biophysical Society

0006-3495/04/01/75/10 \$2.00

observed between the model predictions and the experimentally observed behavior of a mutant virus strain.

Here, we extend the Shea and Ackers (1985) model to account for recently discovered (Dodd et al., 2001; Ptashne and Gann, 2000) interactions (cooperativity) between regulatory molecules bound at two different operator regions. We pay special attention to the estimation of all of the model parameters from published experimental results. An analysis of the model steady states reveals that under normal conditions it only has one stable steady state, corresponding to lysogeny. When the degradation rate of the protein CI is slightly increased from its normal value ( $0.0 \text{ min}^{-1}$ ), two additional steady states appear through a saddle node bifurcation. One of these new steady states is also stable and corresponds to lysis, whereas the other is an (unstable) saddle node. This bistable behavior is maintained with further increases of the CI degradation rate until it reaches  $\sim 0.35 \text{ min}^{-1}$ , when the saddle node and the lysogenic steady state collide and annihilate each other through a reverse saddle node bifurcation. For even larger degradation CI rates there is only one stable steady state, corresponding to lysis. The consequences of these results on the performance and stability of the phage  $\lambda$  switch are finally discussed.

## THE PHAGE $\lambda$ SWITCH

An excellent review of the molecular regulatory mechanisms in the phage  $\lambda$  switch is given by Ptashne (1986). A schematic representation of the  $\lambda$  switch performance in the lysogenic and lytic steady states is shown in Fig. 1. All of the switch regulatory processes take place in the right operator ( $O_R$ ), which is composed of three regions designated  $O_{R1}$ ,  $O_{R2}$ , and  $O_{R3}$ . The promoter  $P_R$  completely overlaps  $O_{R1}$  and partially overlaps  $O_{R2}$ . RNA polymerase enzymes that bind to the promoter  $P_R$  initiate transcription of gene *cro*. Similarly, the promoter  $P_{RM}$  completely overlaps  $O_{R3}$  and partially overlaps  $O_{R2}$ . RNA polymerase enzymes bound to the promoter  $P_{RM}$  initiate transcription of the *cl* gene. Dimers of *cl* product (denoted by  $CI_2$ ) can bind to  $O_{R1}$ ,  $O_{R2}$ , and  $O_{R3}$ , in order of increasing affinity. Conversely, dimers of *cro* product (denoted by  $Cro_2$ ) bind to  $O_{R3}$  with the highest affinity, then to  $O_{R2}$ , and finally to  $O_{R1}$ . When  $CI_2$ 's bind to adjacent  $O_R$  locations, they do so cooperatively. Thus, the binding energy when there are  $CI_2$ 's bound to  $O_{R1}$  and  $O_{R2}$  or to  $O_{R2}$  and  $O_{R3}$  is smaller (larger in absolute value given that interaction and binding energies are negative) than the sum of the individual binding energies. Recently, Darling et al. (2000b) observed that there is also cooperativity between  $Cro_2$ 's bound to  $O_{R1}$  and  $O_{R2}$ , to  $O_{R2}$  and  $O_{R3}$ , and to  $O_{R1}$ ,  $O_{R2}$ , and  $O_{R3}$ . All of the individual-site binding and interaction energies are given in Darling et al. (2000b).

In the lysogenic state (see Fig. 1), gene *cl* is on while gene *cro* is off. Monomers of *cl* product (denoted by CI) spontaneously combine to form dimers  $CI_2$ . Similarly,

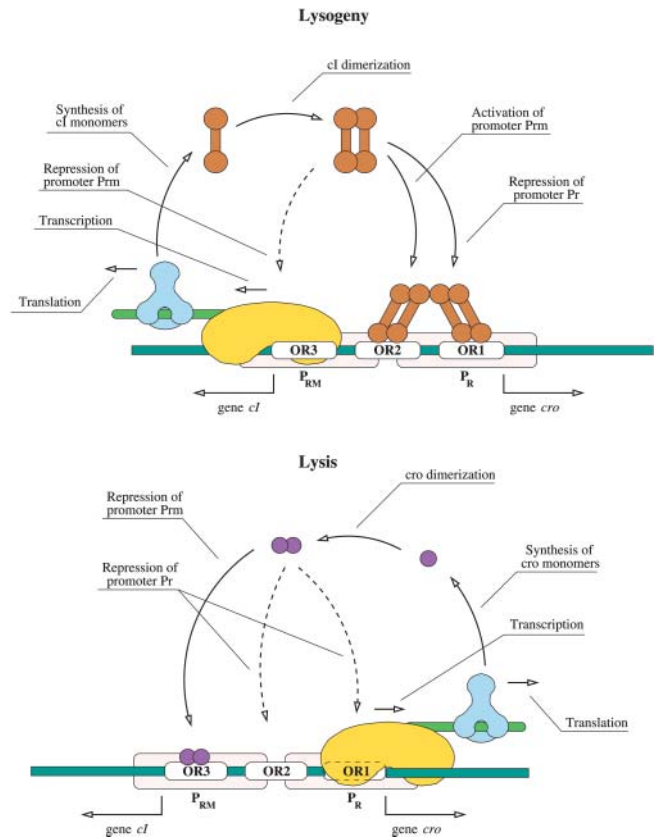


FIGURE 1 A schematic representation of the phage  $\lambda$  switch in the two stable states: lysogeny (top) and lysis (bottom).

monomers of *cro* product (denoted by Cro) spontaneously form dimers  $Cro_2$ . Due to cooperativity, most of the  $O_{R1}$  and  $O_{R2}$  sites are occupied by  $CI_2$ 's in the normal lysogenic state. This has two effects: 1), promoter  $P_R$  is repressed (because it is blocked by a  $CI_2$ ); and 2), the initiation of transcription at promoter  $P_{RM}$  is enhanced. One  $CI_2$  bound to  $O_{R2}$  does not affect the probability that a RNA polymerase will bind promoter  $P_{RM}$  and form a closed complex, but it increases the probability for the closed complex to isomerize into an open complex to start transcription. In other words, dimers  $CI_2$  repress the production of Cro and enhance the production of CI. Nevertheless, if the concentration of  $CI_2$  reaches very high values, the probability for  $CI_2$  to bind  $O_{R3}$  will be increased, which has the effect of repressing RNA polymerase binding to  $P_{RM}$ . Thus  $CI_2$  regulates its own concentration by enhancing CI production if its concentration is not too high, and otherwise repressing transcription of gene *cl*.

If the  $CI_2$  concentration decreases, for instance by the cleavage of CI by RecA proteins (activated by UV light), the probability for  $O_{R1}$  and  $O_{R2}$  to be free from  $CI_2$  is increased. This, on its own, creates the possibility that a polymerase will bind  $P_R$  and start transcription of gene *cro* and, in the long run, leads to an increasing  $Cro_2$  concentration. At a high enough  $Cro_2$  concentration, a  $Cro_2$  can bind  $O_{R3}$  and repress

CI production, establishing the lytic state. In this state, gene *cro* is on while gene *cI* is off. When the concentration of Cro<sub>2</sub> is too high, a Cro<sub>2</sub> can bind to O<sub>R2</sub> and even to O<sub>R1</sub>, repressing the production of Cro.

New experimental evidence (Dodd et al., 2001; Ptashne and Gann, 2000) suggests that there is cooperativity between CI<sub>2</sub>'s bound to the O<sub>R</sub> and O<sub>L</sub> operators. As depicted in Fig. 2, the phage  $\lambda$  DNA folds in such a way that CI<sub>2</sub>'s bound to O<sub>R</sub> and O<sub>L</sub> sites can interact due to their proximity. Ptashne and Gann (2000) speculate that this newly discovered

has three binding states. They can be either free, bound by a CI<sub>2</sub>, or bound by a Cro<sub>2</sub>. The other three states arise because whenever O<sub>L2</sub> and O<sub>L3</sub> are free, a RNA polymerase molecule can bind P<sub>L</sub>, independent of the state of O<sub>L1</sub>.

The energy ( $E_i$ ) of every one of the  $40 \times 30 = 1200$  binding states of the complex formed by the right and left operators plus the promoters P<sub>R</sub>, P<sub>RM</sub>, and P<sub>L</sub> can be calculated given the cooperativity and individual binding energies of CI<sub>2</sub>, Cro<sub>2</sub>, and mRNAP. The equation to calculate these energies is:

$$E_i = \sum_{X=R,L} \sum_{Y=CI_2, Cro_2} \sum_{\nu=1}^3 \Delta G_{O_X^\nu}^Y \Gamma_{O_X^\nu}^Y(i) + \sum_{X=R,L} \sum_{Y=CI_2, Cro_2} \sum_{\nu=1}^2 \Delta G_{O_X^{\nu\nu+1}}^Y \Gamma_{O_X^\nu}^Y(i) \Gamma_{O_X^{\nu+1}}^Y(i) + \sum_{X=R,L} \Delta G_{O_X^{123}}^{Cro_2} \Gamma_{O_X^1}^{Cro_2}(i) \Gamma_{O_X^2}^{Cro_2}(i) \Gamma_{O_X^3}^{Cro_2}(i) \\ + \sum_{X=RM,R,L} \Delta G_{P_X}^{RNAP} \Gamma_{P_X}^{RNAP}(i) + \sum_{\nu=1}^3 \Delta G_{RL} \Gamma_{O_R^\nu}^{CI_2}(i) \Gamma_{O_L^\nu}^{CI_2}(i), \quad (1)$$

cooperativity may help explain the incredibly high stability of the lysogenic state.

## MODEL DEVELOPMENT

The complex formed by the operator O<sub>R</sub> and the promoters P<sub>R</sub> and P<sub>RM</sub> has 40 different binding states. Twenty-seven of these states arise when we consider that O<sub>R1</sub>, O<sub>R2</sub>, and O<sub>R3</sub> can be either empty, bound by a CI<sub>2</sub>, or bound by a Cro<sub>2</sub>, giving  $3^3 = 27$  different possible combinations without considering the binding of RNA polymerase molecules to promoters P<sub>R</sub> and P<sub>RM</sub>. The fact that whenever O<sub>R3</sub> is free (no matter what the  $3^2 = 9$  states of O<sub>R1</sub> and O<sub>R2</sub> are), promoter P<sub>RM</sub> can be bound by a RNA polymerase, accounts for nine more binding states. Similarly, three more states appear because whenever O<sub>R1</sub> and O<sub>R2</sub> are free (regardless of the state of O<sub>R3</sub> (three combinations)), promoter P<sub>R</sub> can be bound by a RNA polymerase. Finally, the last binding state (to complete all 40 of them) is that in which all three O<sub>R1</sub>, O<sub>R2</sub>, and O<sub>R3</sub> are free and both P<sub>R</sub> and P<sub>RM</sub> are occupied by RNA polymerase molecules.

The left operator of phage  $\lambda$  (O<sub>L</sub>) consists of three regions O<sub>L1</sub>, O<sub>L2</sub>, and O<sub>L3</sub>, that can be bound by CI<sub>2</sub> and Cro<sub>2</sub> molecules. There is only one promoter regulated by this operator, promoter P<sub>L</sub>. This promoter completely overlaps O<sub>L1</sub> and partially overlaps O<sub>L2</sub>. Thus, the left operator-P<sub>L</sub> complex has 30 different binding states. Twenty-seven of them arise from the fact that each one of O<sub>L1</sub>, O<sub>L2</sub>, and O<sub>L3</sub>

where

$$\Gamma_X^Y(i) = \begin{cases} 1, & \text{if molecule } Y \text{ is bound to site } X \\ 0, & \text{otherwise} \end{cases}.$$

The terms  $\Delta G_{P_X}^{RNAP}$  ( $X = RM, R, L$ ) represent the binding energy of a RNAP molecule bound to site P<sub>X</sub>, the terms  $\Delta G_{O_X^\nu}^Y$  ( $X = R, L$ ) represent the binding energy of molecule Y to site O<sub>X $\nu$</sub> , the terms  $\Delta G_{O_X^{\nu\nu+1}}^Y$  represent the interaction energy between two Y molecules bound to sites O<sub>X $\nu$</sub>  and O<sub>X $\nu+1$</sub> , and the terms  $\Delta G_{O_X^{123}}^{Cro_2}$  represent the interaction energy between three Cro<sub>2</sub> molecules bound to O<sub>X1</sub>, O<sub>X2</sub>, and O<sub>X3</sub>. All of these individual binding and interaction energies have been measured elsewhere and are given in Appendix A. To our knowledge, the interaction energy between CI<sub>2</sub>'s bound to operators O<sub>R</sub> and O<sub>L</sub> has not yet been measured. The present model assumes that whenever there is one CI<sub>2</sub> bound to O<sub>R $\nu$</sub>  and a second CI<sub>2</sub> is bound to O<sub>L $\nu$</sub> , they interact with an energy  $\Delta G_{RL}$  whose value is also estimated in Appendix A.

Following the same technique used by Ackers et al. (1982) and Shea and Ackers (1985), under the assumption of thermodynamic equilibrium, the probability of every one of the 1200 binding states can be calculated from

$$P_i = \frac{\exp(-E_i/RT) [CI_2]^{\alpha_i} [Cro_2]^{\beta_i} [RNAP]^{\gamma_i}}{Z}. \quad (2)$$

In Eq. 2,  $P_i$  and  $E_i$  are the probability and the energy of the  $i$ -th binding state, respectively.  $R$  is the ideal gas constant and  $T$  is the absolute temperature. Here we take  $T = 37^\circ\text{C}$  so  $RT \simeq 0.617$  kcal/mol (Ackers et al., 1982; Shea and Ackers, 1985). The partition function  $Z$  is given by

$$Z = \sum_i \exp(-E_i/RT) [CI_2]^{\alpha_i} [Cro_2]^{\beta_i} [RNAP]^{\gamma_i}. \quad (3)$$

Finally,  $[CI_2]$ ,  $[Cro_2]$ , and  $[RNAP]$  are, respectively, the concentration of CI<sub>2</sub>, Cro<sub>2</sub>, and RNA polymerase molecules,

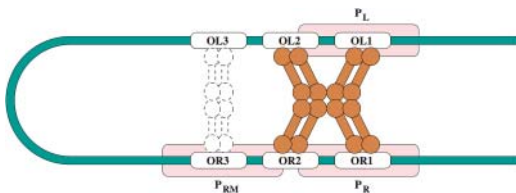


FIGURE 2 Proposed interaction between CI<sub>2</sub>s bound at O<sub>R</sub> and O<sub>L</sub>.

whereas  $\alpha_i$ ,  $\beta_i$ , and  $\gamma_i$  are, respectively, the number of  $CI_2$ ,  $Cro_2$ , and RNA polymerase molecules bound to the operator-promoter complex in the  $i$ -th state.

Note that the thermodynamic equilibrium assumption does not mean that the probabilities remain constant in time. Rather, it means that the probabilities considered are those that would be attained by the real system if it would have enough time to reach the state of thermodynamic equilibrium, given the concentrations  $[CI_2]$ ,  $[Cro_2]$ , and  $[RNAP]$ . If these concentrations are time dependent, the probabilities given under the thermodynamic equilibrium assumption will change accordingly. If the chemical processes involving association and dissociation of  $CI_2$  and  $Cro_2$ , as well as RNA polymerase molecules to the right operator-promoter complex, take place rapidly (relative to the temporal changes of the concentrations  $[CI_2]$ ,  $[Cro_2]$ , and  $[RNAP]$ ), the thermodynamic equilibrium assumption is appropriate.

The probability  $f_R$  for  $P_R$  to be bound by a polymerase can be calculated by adding the probability of all compatible states, i.e., all the states in which a polymerase is bound to  $P_R$  while  $O_{R1}$  and  $O_{R2}$  are free, independent of the states of  $O_{R3}$ ,  $P_{RM}$ ,  $O_{L1}$ ,  $O_{L2}$ ,  $O_{L3}$ , and  $P_L$ . Similarly, the probability  $f_{RM}^q$  for a polymerase to be bound to  $P_{RM}$  with a  $CI_2$  bound to  $O_{R2}$  can be calculated by adding the probability of all the binding states in which  $O_{R3}$  is free, a polymerase is bound to  $P_{RM}$ , and a  $CI_2$  is bound to  $O_{R2}$ , no matter what the states of  $O_{R1}$ ,  $P_R$ ,  $O_{L1}$ ,  $O_{L2}$ ,  $O_{L3}$ , and  $P_L$  are. Finally, the probability  $f_{RM}^s$  for a polymerase to be bound to  $P_{RM}$  without a  $CI_2$  bound to  $O_{R2}$  is calculated by adding the probability of all the states in which  $O_{R3}$  is free, a polymerase is bound to  $P_{RM}$ , and  $O_{R2}$  is either free or bound by a  $Cro_2$  independent of the states of  $O_{R1}$ ,  $P_R$ ,  $O_{L1}$ ,  $O_{L2}$ ,  $O_{L3}$ , and  $P_L$ .

The rate at which RNA polymerase molecules start transcription of the genes  $cro$  and  $cl$  can be written as  $k_{cro}f_R[O_R]$  and  $(k_{cl}^q f_{RM}^q + k_{cl}^s f_{RM}^s)[O_R]$ , respectively (Ackers et al., 1982; Shea and Ackers, 1985).  $k_{cro}$  is the transcription initiation rate constant of promoter  $P_R$ , whereas  $k_{cl}^q$  and  $k_{cl}^s$  are the transcription initiation rate constants of promoter  $P_{RM}$  when  $O_{R2}$  is bound by or free from a  $CI_2$  molecule, respectively.  $O_R$  is the right operator concentration.

Let  $[M_{cl}]$  and  $[M_{cro}]$  be the concentration of  $cl$  and  $cro$  mRNA molecules, respectively. Let  $[CI_T]$  and  $[Cro_T]$ , respectively, denote the total concentration of CI and Cro monomers. These concentrations are calculated by adding the free monomer plus twice the dimer concentrations. Thus, from the considerations in the previous paragraphs, we propose the following equations to model the dynamic evolution of  $[M_{cl}]$ ,  $[M_{cro}]$ ,  $[CI_T]$ , and  $[Cro_T]$ :

$$\begin{aligned} \frac{d[M_{cl}]}{dt} = & k_{cl}^q [O_R] f_{RM}^q ([CI_2]_{\tau_M}, [CI_2]_{\tau_M}) \\ & + k_{cl}^s [O_R] f_{RM}^s ([CI_2]_{\tau_M}, [Cro_2]_{\tau_M}) - (\gamma_M + \mu) [M_{cl}], \end{aligned} \quad (4)$$

$$\frac{d[M_{cro}]}{dt} = k_{cro} [O_R] f_R ([CI_2]_{\tau_M}) - (\gamma_M + \mu) [M_{cro}], \quad (5)$$

$$\frac{d[CI_T]}{dt} = v_{cl} [M_{cl}]_{\tau_{cl}} - (\gamma_{cl} + \mu) [CI_T], \quad (6)$$

and

$$\frac{d[Cro_T]}{dt} = v_{cro} [M_{cro}]_{\tau_{cro}} - (\gamma_{cro} + \mu) [Cro_T]. \quad (7)$$

The meaning of all parameters appearing for the first time in these equations is as follows:  $\gamma_M$  is the rate of mRNA degradation;  $\gamma_{cro}$  is the rate of  $Cro_T$  degradation;  $\gamma_{cl}$  is the rate of  $CI_T$  degradation;  $\tau_M$  is time required after transcription initiation to have a mRNA ready to be bound by a ribosome;  $\tau_{cl}$  is the time it takes to translate a monomer CI;  $\tau_{cro}$  is the time it takes to translate a monomer Cro;  $v_{cl}$  is the rate of  $cl$  translation initiation; and  $v_{cro}$  is the rate of  $cro$  translation initiation. The notation  $X_\tau$  means  $X_\tau \equiv X(t - \tau)$ .

The dimer concentrations ( $[CI_2]$  and  $[Cro_2]$ ) can be calculated in terms of the total monomer concentrations ( $[CI_T]$  and  $[Cro_T]$ ) if we make a quasi-steady-state assumption for the dimerization reactions (see Appendix B):

$$[CI_2] = \frac{1}{2} [CI_T] - \frac{K_D^{cl}}{8} \left[ \sqrt{1 + 8 \frac{[CI_T]}{K_D^{cl}}} - 1 \right], \quad (8)$$

and

$$[Cro_2] = \frac{1}{2} [Cro_T] - \frac{K_D^{cro}}{8} \left[ \sqrt{1 + 8 \frac{[Cro_T]}{K_D^{cro}}} - 1 \right], \quad (9)$$

where  $K_D^{cl}$  and  $K_D^{cro}$ , respectively, denote the CI and Cro dimerization dissociation constants.

The values of all of the parameters in Eq. 4–9 are estimated in Appendix A and tabulated in Table 1.

## NUMBER AND LOCATION OF THE STEADY STATES

The model given by Eq. 4–9 reaches a steady state whenever  $d[M_{cl}]/dt = 0$ ,  $d[M_{cro}]/dt = 0$ ,  $d[CI_T]/dt = 0$ , and  $d[Cro_T]/dt = 0$ . Given that, in the steady state, all of the delayed variables attain their steady-state value, the time delays  $\tau_M$ ,  $\tau_{cl}$ , and  $\tau_{cro}$  may be ignored. It can be shown after a little

**TABLE 1** Estimated values for the parameters in Eq. 4–9

$\mu \simeq 2.0 \times 10^{-2} \text{ min}^{-1}$	$k_{cro} \simeq 2.76 \text{ min}^{-1}$
$k_{cl}^q \simeq 4.29 \text{ min}^{-1}$	$k_{cl}^s \simeq 0.35 \times \text{min}^{-1}$
$\gamma_M \simeq 0.12 \text{ min}^{-1}$	$\gamma_{cl} \simeq 0.0 \text{ min}^{-1}$
$\gamma_{cro} \simeq 1.6 \times 10^{-2} \text{ min}^{-1}$	$v_{cl} \simeq 0.09 \text{ min}^{-1}$
$v_{cro} \simeq 3.2 \text{ min}^{-1}$	$\tau_{cl} \simeq 0.24 \text{ min}$
$\tau_{cro} \simeq 6.6 \times 10^{-2} \text{ min}$	$\tau_M \simeq 5.1 \times 10^{-3} \text{ min}$
$K_D^{cl} \simeq 5.56 \times 10^{-3} \mu\text{M}$	$K_D^{cro} \simeq 3.26 \times 10^{-1} \mu\text{M}$
$[O_R] \simeq 5.0 \times 10^{-3} \mu\text{M}$	$[mRNAP] \simeq 3.0 \mu\text{M}$
$\Delta G_{RL} \simeq -3.1 \text{ kcal/mol}$	

algebra that the  $CI_T$  and  $Cro_T$  steady-state values satisfy the following equations:

$$\Phi([CI_T], [Cro_T], \gamma_{cl}) = 0, \quad (10)$$

and

$$\Theta([CI_T], [Cro_T]) = 0, \quad (11)$$

where

$$\Phi([CI_T], [Cro_T], \gamma_{cl}) = \frac{v_{cl}}{\gamma_M + \mu} [O_R] (k_{cl}^q f_{RM}^q + k_{cl}^s f_{RM}^s) - (\gamma_{cl} + \mu) [CI_T], \quad (12)$$

and

$$\Theta([CI_T], [Cro_T]) = \frac{v_{cro}}{\gamma_M + \mu} [O_R] k_{cro} f_R - (\gamma_{cro} + \mu) [Cro_T]. \quad (13)$$

The equation  $\Phi([CI_T], [Cro_T], \gamma_{cl}) = 0$  determines a family of curves in the  $([CI_T], [Cro_T])$  space (one for every value of  $\gamma_{cl}$ ), whereas the equation  $\Theta([CI_T], [Cro_T]) = 0$  determines one single curve in the same space. For a given value of  $\gamma_{cl}$ , the points where the curves  $\Phi = 0$  and  $\Theta = 0$  intersect correspond to the steady states of the system.

The curve  $\Theta = 0$  is shown in Fig. 3 in the  $[Cro_T]$  vs.  $[CI_T]$  phase space, along with  $\Phi = 0$  curves for various values of  $\gamma_{cl}$ . For the normal lysogenic value  $\gamma_{cl} \simeq 0.0 \text{ min}^{-1}$  (see Table 1), both curves intersect at only one point implying that for this value of  $\gamma_{cl}$  there is only one steady state. This steady state is stable (this point is discussed below in more detail) and corresponds to the lysogenic steady state. Nevertheless, this behavior is at the verge of a bifurcation because a slight increment of  $\gamma_{cl}$  makes the curve  $\Phi = 0$  tangentially intersect the curve  $\Theta = 0$ . At this point, two more steady states appear via a saddle node bifurcation. One of these steady states is stable and corresponds to the lytic

state (see below for more detail), whereas the other is a saddle node. With further increases in  $\gamma_{cl}$ , the lytic steady state separates from the saddle node, and the saddle node approaches the lysogenic steady state. When  $\gamma_{cl}$  reaches a value of  $\sim 0.35 \text{ min}^{-1}$ , the saddle node and the lysogenic state collide and annihilate through a reverse saddle node bifurcation.

## NUMERICAL TEST OF THE STEADY STATES' STABILITY PROPERTIES

Consider the system of time-delay differential equations given by Eq. 4–7. In Table 1, it is clear that the time delay  $\tau_M$  is one order of magnitude smaller than  $\tau_{cl}$  and two orders of magnitude smaller than  $\tau_{cro}$ . This observation allows us to slightly simplify the model by ignoring the time delay  $\tau_M$  wherever it appears. After this simplification, the system of equations was numerically solved by means of the fourth-order Runge-Kutta algorithm (adapted to account for the time delays), implemented in FORTRAN.

Projections of the phase space trajectories onto the  $([CI_T], [Cro_T])$  space are shown in Fig. 4 for various values of  $\gamma_{cl}$ . The curves in this figure exemplify a large amount of numerical experiments that we performed to test the steady states' stability properties. These properties can be described as follows: for  $\gamma_{cl} = 0.0 \text{ min}^{-1}$  the system has one single globally stable steady state corresponding to lysogeny (Fig. 4 A). A slight increment of  $\gamma_{cl}$  beyond this value produces two more steady states via a saddle node bifurcation. One of these is stable and corresponds to lysis whereas the other is an unstable saddle node (Fig. 4 B). This bistable behavior is maintained with further increments of  $\gamma_{cl}$  until about  $\gamma_{cl} \simeq 0.35 \text{ min}^{-1}$ , when the saddle node and the lysogenic steady state collide annihilating each other by means of a reverse saddle node bifurcation. For  $\gamma_{cl}$ 's larger than  $0.35 \text{ min}^{-1}$

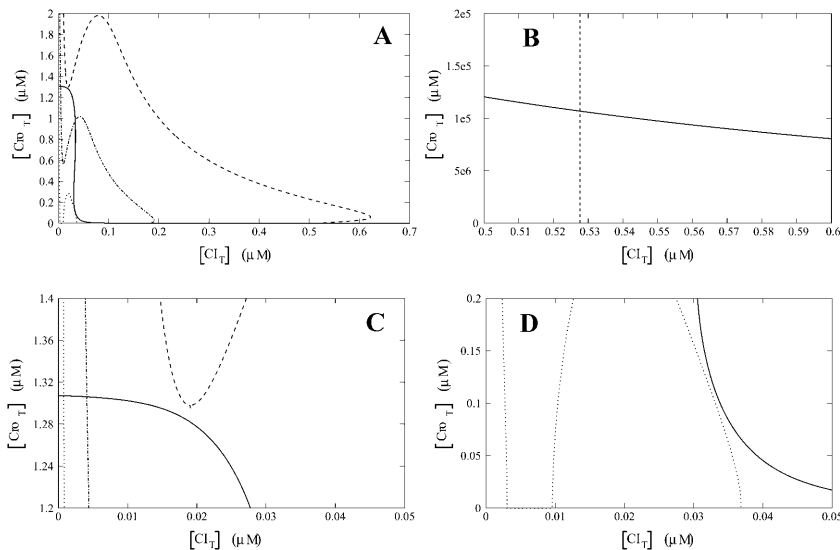


FIGURE 3 Plots in the  $[Cro_T]$  vs.  $[CI_T]$  plane of the  $\Theta = 0$  curve (solid line) and of the  $\Phi = 0$  curves for various values of  $\gamma_{cl}$ : the dashed line corresponds to  $\gamma_{cl} = 0.0 \text{ min}^{-1}$ , the dot-dashed line corresponds to  $\gamma_{cl} = 0.05 \text{ min}^{-1}$ , and the dotted curve corresponds to  $\gamma_{cl} = 0.35 \text{ min}^{-1}$ . Intersections between the  $\Theta = 0$  and  $\Phi = 0$  plots locate the system steady states. The whole curves are shown in A. In B, the lysogenic steady state corresponding to  $\gamma_{cl} = 0$  is shown, whereas in C and D we show zooms of the regions where the bifurcations take place. All these curves were numerically calculated with the aid of Octave's algorithm "fsolve."

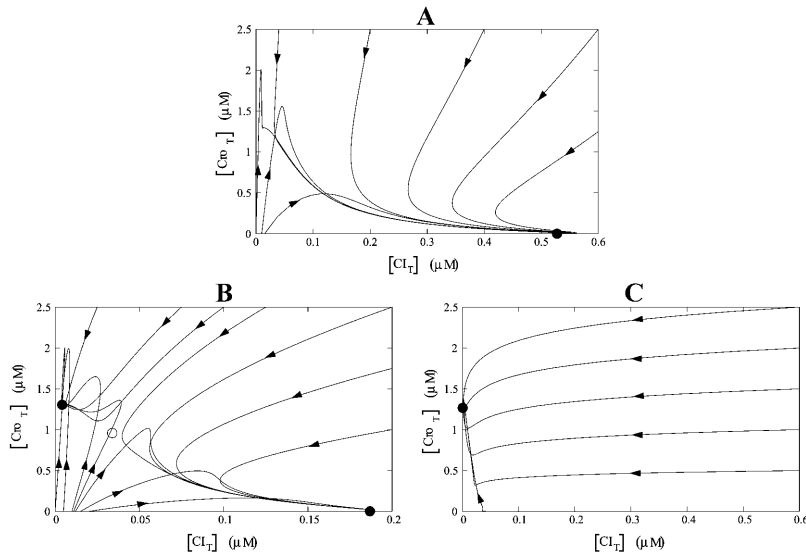


FIGURE 4 Projections onto the  $([CI_T], [Cro_T])$  space of the phase space trajectories (derived from the numerical solutions of the system time-delay differential equations, for various initial conditions) of the phage  $\lambda$  switch model for different values of  $\gamma_{cl}$ : (A)  $\gamma_{cl} = 0.0 \text{ min}^{-1}$ , (B)  $\gamma_{cl} = 0.05 \text{ min}^{-1}$ , and (C)  $\gamma_{cl} = 0.35 \text{ min}^{-1}$ . Note that the tangled appearance of the trajectories in A and B are due to the projection from a four-dimensional phase space into the plane. Stable steady states are indicated with filled circles, whereas unstable steady states, if any, are indicated with empty circles.

the system has one single globally stable lytic steady state (Fig. 4 C).

We numerically solved the model equations by changing the value of parameters other than  $\gamma_{cl}$  to test the robustness of our results. We found that of all the parameters, the model is particularly sensitive to changes in  $\Delta G_{RL}$ . Indeed, for absolute values of  $\Delta G_{RL}$ 's smaller than 3.1 kcal/mol the system shows a bistable behavior even for  $\gamma_{cl} = 0.0 \text{ min}^{-1}$ . When the absolute value of  $\Delta G_{RL}$  is increased beyond 3.1 kcal/mol, the system has one single steady state (corresponding to lysogeny) for  $\gamma_{cl} = 0.0 \text{ min}^{-1}$ , and the values of  $\gamma_{cl}$  at which the bifurcations take place increase. This behavior is pictured as a bifurcation diagram in Fig. 5. The above described results indicate that cooperativity between the right and left operator regions plays a very important role in the stability of the lysogeny steady state. Moreover, they also

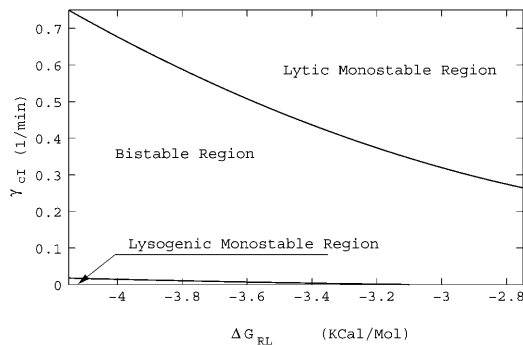


FIGURE 5 Bifurcation diagram in the  $(\Delta G_{RL}, \gamma_{cl})$  parameter space. Three different qualitative dynamic behaviors, which correspond to the three regions illustrated in the bifurcation diagram, can be observed: either the system has one single stable steady state corresponding to lysogeny, it has only one stable steady state corresponding to lysis, or it has three steady states, two of them being stable (the lysogenic and lytic states) and the other being a saddle node. The boundaries between the three regions identify the values of  $\Delta G_{RL}$  and  $\gamma_{cl}$  at which the bifurcations take place.

highlight the necessity of detailed experiments to clarify the nature of the interaction between CI dimers bound to the left and right operator regions.

Some of the estimated parameters were obtained by averaging previously reported values. In some cases, the relative errors are higher than 30%. This is in particular the case with  $k_{cl}^s \in [0.3, 0.41] \text{ min}^{-1}$  and  $k_{cl}^q \in [3.42, 5.16] \text{ min}^{-1}$ . To test how this variability affects the system dynamic behavior we redraw the plots of Fig. 3 (which illustrate the number and location of the system's steady states for different values of  $\gamma_{cl}$ ) using the extreme values of the  $P_{RM}$  transcription initiation rates  $k_{cl}^s$  and  $k_{cl}^q$ . These plots are presented in Fig. 6. There, notice that with the lowest  $k_{cl}^s$  and  $k_{cl}^q$  values, the system shows bistability even for  $\gamma_{cl} = 0 \text{ min}^{-1}$ . Moreover, the  $\gamma_{cl}$  value at which the lysogenic steady state and the saddle node collide and annihilate decreases. A comparison with the bifurcation diagram of Fig. 5 reveals that the only effect of decreasing the values of  $k_{cl}^s$  and  $k_{cl}^q$  is to slightly displace the bifurcation curves of Fig. 5 to the left along the  $\Delta G_{RL}$  axis. Similarly, increasing the  $k_{cl}^s$  and  $k_{cl}^q$  values has the single effect of slightly displacing the bifurcation curves to the right. Thus, we conclude that changes of parameters  $k_{cl}^s$  and  $k_{cl}^q$  even larger than 30% do not alter the overall qualitative dynamic behavior of the system.

## CONCLUSIONS

Our results provide a possible answer to the question of why the lysogenic steady state is so stable. Namely, from our model and analysis the phage  $\lambda$  switch has only one steady state under normal conditions. Moreover, based on our numerical results the lysogeny steady state appears to be globally stable. This is in agreement with the fact that the lysogenic state is even more stable than the genome itself. Only that fraction of mutations that typically increase the CI degradation rate can cause some lysogens to become lytic.

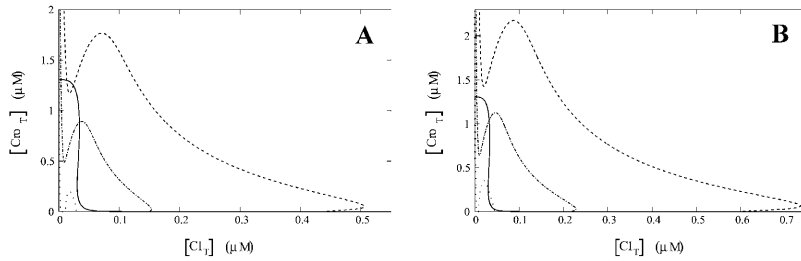


FIGURE 6 Plots in the  $[Cro_T]$  vs.  $[CI_T]$  plane of the  $\Theta = 0$  curve (solid line) and of the  $\Phi = 0$  curves for various values of  $\gamma_{CI}$ : the dashed line corresponds to  $\gamma_{CI} = 0.0 \text{ min}^{-1}$ , the dot-dashed line corresponds to  $\gamma_{CI} = 0.05 \text{ min}^{-1}$ , and the dotted curve corresponds to  $\gamma_{CI} = 0.35 \text{ min}^{-1}$ . Intersections between the  $\Theta = 0$  and  $\Phi = 0$  plots locate the system steady states. The plots in A and B were calculated, respectively, with the smallest and largest values of  $k_{CI}^S$  and  $k_{CI}^L$  reported in the literature.

Conversely, if after being irradiated with UV light the activated RecA proteins cleave CI monomers at a rate  $>0.35 \text{ min}^{-1}$ , all of the infected bacteria will go into lysis. This will happen because lysis will be the only available steady state, which is globally stable under this condition. Thus, by taking into account the cooperativity between  $CI_2$ 's bound at the  $O_R$  and  $O_L$  operators, it is possible to explain the astonishingly high stability of the phage  $\lambda$  lysogenic state, as well as the almost perfect efficiency of the switch.

The estimated energy of interaction between  $CI_2$ 's bound to the left and right operators ( $\Delta G_{RL}$ ), relies on an assumed interaction that has not been experimentally demonstrated. Nevertheless, we believe our model is robust in this respect based on the fact that the value we estimate for  $\Delta G_{RL}$  is similar to the measured interaction energy between  $CI_2$ 's bound to adjacent  $O_R$  sites (see Appendix A). Furthermore, our assumption can be tested experimentally.

In this work, we predict bistable behavior (between the lysogenic and lytic states) for CI degradation rates ( $\gamma_{CI}$ ) larger than 0.0 but smaller than  $0.35 \text{ min}^{-1}$ . To test this prediction, mutant phage  $\lambda$  strains in which CI is not as stable as it is in the wild type would be useful. If for such mutant strains  $\gamma_{CI}$  is large enough to induce bistable behavior, a rate of lysogen loss of the same order of magnitude as that predicted by Arkin et al. (1998) should be observed, instead of the (orders of magnitude smaller) wild-type loss rate. Other possible tests of the model would involve mutant *E. coli* strains, in which the activated RecA proteins fail to cleave CI at a rate high enough to induce one single lytic stable steady state. Then, the system would still be in the bistable region, and some of the lysogens would always survive after having been irradiated with UV light.

The dynamic influence of the thermodynamic equilibrium approximation, on which this and other models rely, should be analyzed. In our particular case, this approximation is equivalent to a quasi-steady-state assumption for the chemical reactions by means of which  $CI_2$ ,  $Cro_2$ , and RNA polymerase molecules bind to, and detach from, the promoter-operator regions. Its validity relies upon the assumption that those chemical reactions are rapid, relative to the transcription and translation processes. In other words, the feasibility of a thermodynamic equilibrium (or a quasi-steady-state) assumption is a question of having phenomena with orders-of-magnitude different characteristic times. In our opinion, although it is not plausible that a phenomono-

logical model based on a thermodynamic equilibrium approximation will generally work for living biological systems, it seems to work well here because the required difference in characteristic times is fulfilled.

The model here presented does not allow us to make quantitative predictions concerning the lysogen loss and survival rates of wild-type and mutant  $\lambda$  strains, under different experimental conditions. To make them, the fluctuations inherent to molecular systems should be accounted for in a stochastic model.

Finally, we call attention to the fact that the model is highly sensitive to changes in the parameter  $\Delta G_{RL}$ . This indicates that the interaction between CI dimers bound to the left and right operator regions plays an important role in the stability of the lysogeny state. However, it also highlights the necessity of detailed experiments concerning this interaction to validate our results.

## APPENDIX A: PARAMETER ESTIMATION

The  $CI_2$  and  $Cro_2$  binding energies to  $O_{R1}$ ,  $O_{R2}$ , and  $O_{R3}$ , the interaction energy between  $CI_2$ 's or  $Cro_2$ 's bound to adjacent sites, and the RNA polymerase binding energy to  $P_R$  and  $P_{RM}$  have been measured elsewhere. The most recent, and presumably most accurate, values are reported by Darling et al. (2000b) and tabulated in Table 2.

**TABLE 2 Binding energies of  $CI_2$  and  $Cro_2$  to  $O_{R1}$ ,  $O_{R2}$ , and  $O_{R3}$  ( $\Delta G_{O_{Ri}}^{CI_2}$  and  $\Delta G_{O_{Ri}}^{Cro_2}$ ,  $i = 1,2,3$ ), interaction energies between adjacent  $CI_2$ 's or  $Cro_2$ 's ( $\Delta G_{O_{Rij}}^{CI_2}$ ,  $\Delta G_{O_{Rij}}^{Cro_2}$ , and  $\Delta G_{O_{R123}}^{Cro_2}$ ,  $i < j$ ) (in this case the dimer-operator binding energies are not considered), and RNA polymerase (RNAP) binding energies to  $P_R$  and  $P_{RM}$  ( $\Delta G_{P_R}^{RNAP}$  and  $\Delta G_{P_{RM}}^{RNAP}$ )**

$\Delta G_{O_{R1}}^{CI_2} \approx -12.5 \text{ kcal/mol}$
$\Delta G_{O_{R2}}^{CI_2} \approx -10.5 \text{ kcal/mol}$
$\Delta G_{O_{R3}}^{CI_2} \approx -9.5 \text{ kcal/mol}$
$\Delta G_{O_{R12}}^{CI_2} \approx -2.7 \text{ kcal/mol}$
$\Delta G_{O_{R23}}^{CI_2} \approx -2.9 \text{ kcal/mol}$
$\Delta G_{O_{R1}}^{Cro_2} \approx -12.0 \text{ kcal/mol}$
$\Delta G_{O_{R2}}^{Cro_2} \approx -10.8 \text{ kcal/mol}$
$\Delta G_{O_{R3}}^{Cro_2} \approx -13.4 \text{ kcal/mol}$
$\Delta G_{O_{R12}}^{Cro_2} \approx -1.0 \text{ kcal/mol}$
$\Delta G_{O_{R23}}^{Cro_2} \approx -0.6 \text{ kcal/mol}$
$\Delta G_{O_{R123}}^{Cro_2} \approx -0.9 \text{ kcal/mol}$
$\Delta G_{P_R}^{RNAP} \approx -12.5 \text{ kcal/mol}$
$\Delta G_{P_{RM}}^{RNAP} \approx 11.5 \text{ kcal/mol}$

The  $Cl_2$  and  $Cro_2$  single-site binding energies at  $O_L$  are reported by Aurell and Sneppen (2002). However, these energies were measured before the cooperativity between  $Cro_2$ 's bound to adjacent sites was discovered.  $Cro_2$  single-site binding energies at  $O_R$  reported before and after cooperativity was discovered are very different. This is not the case with  $Cl_2$  (Darling et al., 2000b). Moreover,  $Cro_2$  single-site binding energies at  $O_R$ , that also ignore cooperativity, are very similar to those of  $O_L$  (Aurell et al., 2002). From this, we take the  $Cl_2$  single-site binding energies reported by Aurell and Sneppen (2002), but for the  $Cl_2$  cooperativity and  $Cro_2$  single-site binding and cooperativity energies at  $O_L$  we assume that they are equal to those of  $O_R$ . Giladi et al. (1990) measured the association constant of the polymerase- $P_L$  closed complex formation. They report a value of  $K_B \simeq 8.94 \times 10^7 \text{ mol}^{-1}$ . From this and taking  $RT \simeq 0.617 \text{ kcal/mol}$ , we can estimate the RNA polymerase- $P_L$  binding energy to be  $\Delta G_{P_L}^{RNAP} = -RT \ln(K_B) \simeq -11.3 \text{ kcal/mol}$ . These energies are tabulated in Table 3.

The value of the probabilities  $f_R^q$ ,  $f_{RM}^q$ , and  $f_{RM}^s$  can be calculated for every value of  $[Cl_2]$  and  $[Cro_2]$  from the energy values tabulated in Tables 2 and 3, as well as from the energy  $\Delta G_{RL}$  and the RNA polymerase concentration  $[RNAP]$  (the last two parameters are estimated below). We also need estimates for the right operator concentration  $[O_R]$ , the growth rate  $\mu$ , the degradation rates  $\gamma_M$ ,  $\gamma_{cl}$ , and  $\gamma_{cro}$ , the transcription initiation rates  $k_{cl}^q$ ,  $k_{cl}^s$ , and  $k_{cro}$ , and for the translation initiation rates  $v_{cl}$  and  $v_{cro}$ .

## Growth rate

Reinitz and Vaisnys (1990) and Little et al. (1999) performed experiments on the shift of the phage  $\lambda$  switch from the lysogeny to the lytic state. In these experiments, they employ a bacterial generation time of  $\sim 34 \text{ min}$ . For the purpose of the present work, we will consider the same generation time, which corresponds to a growth rate of  $\mu \simeq 2.0 \times 10^{-2} \text{ min}^{-1}$ .

## *E. coli* volume

*E. coli* are rodlike bacteria 3–5  $\mu\text{m}$  long and 0.5  $\mu\text{m}$  in diameter, so they have a volume in the range from  $6.0 \times 10^{-16} \text{ L}$  to  $9.8 \times 10^{-16} \text{ L}$ . We considered a mean volume of  $8.0 \times 10^{-16} \text{ L}$ .

## RNA polymerase concentration $[RNAP]$

According to Bremer and Dennis (1996), there are  $\sim 1,500$  RNA active polymerase molecules per cell in *E. coli* bacterial cultures growing at the rate  $\mu$  as estimated above. This leads to a concentration  $[RNAP] \simeq 3.0 \mu\text{M}$ .

**TABLE 3** Energies of  $Cl_2$  and  $Cro_2$  binding to  $O_{L1}$ ,  $O_{L2}$ , and  $O_{L3}$  ( $\Delta G_{O_{L,i}}^{Cl_2}$  and  $\Delta G_{O_{L,i}}^{Cro_2}$ ,  $i = 1,2,3$ ), interaction energies between adjacent  $Cl_2$ 's or  $Cro_2$ 's ( $\Delta G_{O_{L,ij}}^{Cl_2}$ ,  $\Delta G_{O_{L,ij}}^{Cro_2}$ , and  $\Delta G_{O_{L,123}}^{Cro_2}$ ,  $i < j$ ) (in this case the dimer-operator binding energies are not considered), and energies of RNA polymerase (RNAP) binding to  $P_L$  ( $\Delta G_{P_L}^{RNAP}$ )

$\Delta G_{O_{L1}}^{Cl_2} \simeq -11.5 \text{ kcal/mol}$
$\Delta G_{O_{L2}}^{Cl_2} \simeq -9.7 \text{ kcal/mol}$
$\Delta G_{O_{L3}}^{Cl_2} \simeq -9.7 \text{ kcal/mol}$
$\Delta G_{O_{L12}}^{Cl_2} \simeq -2.7 \text{ kcal/mol}$
$\Delta G_{O_{L23}}^{Cl_2} \simeq -2.9 \text{ kcal/mol}$
$\Delta G_{O_{L1}}^{Cro_2} \simeq -12.0 \text{ kcal/mol}$
$\Delta G_{O_{L2}}^{Cro_2} \simeq -10.8 \text{ kcal/mol}$
$\Delta G_{O_{L3}}^{Cro_2} \simeq -13.4 \text{ kcal/mol}$
$\Delta G_{O_{L12}}^{Cro_2} \simeq -1.0 \text{ kcal/mol}$
$\Delta G_{O_{L23}}^{Cro_2} \simeq -0.6 \text{ kcal/mol}$
$\Delta G_{O_{L123}}^{Cro_2} \simeq -0.9 \text{ kcal/mol}$
$\Delta G_{P_L}^{RNAP} \simeq -11.3 \text{ kcal/mol}$

## Right operator concentration $[O_R]$

According to Bremer and Dennis (1996), there are  $\sim 2.5$  genome equivalents per average *E. coli* cell at the growth rate determined by  $\mu$ . Assuming one operator  $O_R$  per genome equivalent, the right operator concentration can be estimated as  $[O_R] \simeq 5.0 \times 10^{-3} \mu\text{M}$ .

## Average lysogenic $Cl_T$ concentration

According to Ptashne (1986), there are between 200 and 350 CI molecules per cell (in monomer units) in lysogenic bacteria. Here, we take the mean number 275, which corresponds to a concentration of  $[Cl_T]_{\text{lysogeny}} \simeq 0.55 \mu\text{M}$ .

## $P_R$ transcription initiation rate $k_{cro}$

Hawley et al. (1985) and Fong et al. (1994) report measurements of the closed-to-open complex isomerization rate at the  $P_R$  operator  $k_{cro}$ . The values they report are respectively:  $k_{cro} \simeq 5.0 \times 10^{-2} \text{ s}^{-1}$  and  $k_{cro} \simeq 4.12 \times 10^{-2} \text{ s}^{-1}$ . We take the mean value  $k_{cro} \simeq 4.6 \times 10^{-2} \text{ s}^{-1} \simeq 2.76 \text{ min}^{-1}$ .

## $P_{RM}$ transcription initiation rates $k_{cl}^q$ and $k_{cl}^s$

Hwang et al. (1988) and Li et al. (1997) report measurements of the closed-to-open complex isomerization rate at the  $P_{RM}$  operator. According to Hwang et al. (1988), this rate in the absence of  $Cl_2$  repressor is around  $k_{cl}^s \simeq 0.68 \times 10^{-2} \text{ s}^{-1}$  and  $k_{cl}^q \simeq 5.7 \times 10^{-2} \text{ s}^{-1}$  in the presence of  $Cl_2$  repressor. Li et al. (1997) report the following values:  $k_{cl}^s \simeq 0.5 \times 10^{-2} \text{ s}^{-1}$  and  $k_{cl}^q \simeq 8.6 \times 10^{-2} \text{ s}^{-1}$ . We consider here the mean values:  $k_{cl}^s \simeq 0.59 \times 10^{-2} \text{ s}^{-1} \simeq 0.35 \text{ min}^{-1}$  and  $k_{cl}^q \simeq 7.15 \times 10^{-2} \text{ s}^{-1} \simeq 4.29 \text{ min}^{-1}$ .

## mRNA degradation rate $\gamma_M$

Court et al. (1980) performed experiments to measure the half-life of  $P_L$  transcripts. They report  $\tau_{1/2} \simeq 6 \text{ min}$ , and assert that the half-lives of the  $P_R$  and  $P_{RM}$  transcripts are similar. From this, the mRNA degradation rate can be estimated to be  $\gamma_M = \ln 2/\tau_{1/2} \simeq 0.12 \text{ min}^{-1}$ .

## $Cl_T$ degradation rate $\gamma_{cl}$

Following Hawley et al. (1985), Reinitz and Vaisnys (1990), Aurell et al. (2002), and Aurell and Sneppen (2002), we ignore the degradation rate of  $Cl_T$  because it is very small compared with other rates in the model, e.g., the growth rate  $\mu$ . Therefore, we take  $\gamma_{cl} = 0$ .

## $Cro_T$ degradation rate $\gamma_{cro}$

Pakula et al. (1986) measured a Cro half-life in vivo of  $\sim 2600 \text{ s} \simeq 43.3 \text{ min}$ . From this,  $\gamma_{cro} \simeq 1.6 \times 10^{-2} \text{ min}^{-1}$ .

## *cl* translation initiation rate $v_{cl}$

Under normal conditions, the system of time-delay differential equations (Eq. 4–7) model has one single stable steady state corresponding to lysogeny. In this lysogenic state,  $P_R$  is very tightly repressed whereas  $P_{RM}$  is repressed only  $\approx 20\%$  (Dodd et al., 2001; Meyer et al., 1980). Because  $k_{cl}^q > k_{cl}^s$ , the maximum activity of the promoter  $P_{RM}$  corresponds to  $f_{RM}^q = 1$  and  $f_{RM}^s = 0$  and is given by  $k_{cl}^q/[O_R]$ . Thus, the normalized activity of the promoter  $P_{RM}$  in the lysogenic state is  $f_{RM}^q + k_{cl}^s/k_{cl}^q f_{RM}^s = 0.8$ , with which the dynamic equation for  $[M_{cl}]$  becomes



$$\frac{d[M_{cl}]}{dt} = 0.8k_{cl}^q - (\gamma_M + \mu)[M_{cl}].$$

By solving for the *cl* translation initiation rate  $v_{cl}$  from this last equation and the dynamic equation for  $[M_{cro}]$ , and taking into account that the concentration of all chemical species is constant in a steady state ( $d[M_{cl}]/dt = 0$  and  $d[CI_T]/dt = 0$ ), we obtain

$$v_{cl} = \frac{(\gamma_{cl} + \mu)(\gamma_M + \mu) [CI_{lysogeny}]}{0.8k_{cl}^q [O_R]} \simeq 0.09 \text{ min}^{-1}.$$

### *cro* translation initiation rate $v_{cro}$

Aurell et al. (2002) estimate that, when translated, a *cro* transcript produces 51% of the polypeptides an ideal *lacZ* transcript produces. From this and taking into account that ribosomes load onto *lacZ* transcripts at  $3.2 \text{ s} = 5.33 \times 10^{-2} \text{ min}$  intervals (Kennell and Riezman, 1977), that the *lacZ* transcript half-life is  $\sim 2 \text{ min}$  (Leive and Kollin, 1967), and that the *cro* transcript half-life is of the order of 6 min (Court et al., 1980), the *cro* translation initiation rate can be estimated as  $v_{cro} \simeq (0.51 \times 2 \text{ min}) / (6 \text{ min} \times 5.33 \times 10^{-2} \text{ min}) \simeq 3.2 \text{ min}^{-1}$ .

### The time delays due to *cl* and *cro* translation

#### $\tau_{cl}$ and $\tau_{cro}$

CI and Cro are proteins that are 267 and 66 amino-acid-long, respectively. This means that gene *cl* is 711 basepairs long, whereas *cro* gene is 198 basepairs long. From this and taking into account that, according to Bremer and Dennis (1996), the mRNA chain elongation rate is  $\sim 50$  nucleotide/s, the time it takes for genes *cl* and *cro* to be translated is  $\tau_{cl} \simeq 0.24 \text{ min}$  and  $\tau_{cro} \simeq 6.6 \times 10^{-2} \text{ min}$ , respectively.

### The time delay due to transcription $\tau_M$

Once a RNA polymerase has transcribed a mRNA chain long enough for a ribosome to bind to it, translation can start. According to Draper (1996), efficient mRNA's can initiate translation every 3 s. From this and the fact that the mRNA chain elongation rate is of the order of 50 nucleotide/s (Bremer and Dennis, 1996),  $< 150$  nucleotides are required for a ribosome to bind a mRNA and start translation. Furthermore, the DNA chain elongation rate is at least 490 nucleotide/s (Bremer and Dennis, 1996). Thus it takes  $< 0.31 \text{ s}$  after transcription initiation to have a mRNA ready for translation initiation. i. e.,  $\tau_M \simeq 5.1 \times 10^{-3} \text{ min}$ .

### The CI and Cro dimerization dissociation constants $K_D^{cl}$ and $K_D^{cro}$

Burz et al. (1994) measured the CI dimerization dissociation constant obtaining  $K_D^{cl} \simeq 5.56 \times 10^{-3} \mu\text{M}$ . The Cro dimerization dissociation constant was measured by Darling et al. (2000a) to give  $K_D^{cro} \simeq 3.26 \times 10^{-1} \mu\text{M}$ .

### Interaction energy between $CI_2$ dimers bound to $O_R$ and $O_L$ , $\Delta G_{RL}$

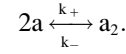
According to Meyer et al. (1980) and Dodd et al. (2001),  $P_R$  is very tightly repressed whereas  $P_{RM}$  is repressed only  $\simeq 20\%$  in the lysogenic state. From this, the  $P_{RM}$  transcription initiation rate  $k_{cl}^q [O_R] f_{RM}^q + k_{cl}^s [O_R] f_{RM}^s$  should be 80% of the maximum transcription initiation rate  $k_{cl}^q [O_R]$ . That is,  $f_{RM}^q + k_{cl}^s / k_{cl}^q f_{RM}^s = 0.8$ . After substitution of the steady state  $[CI_T] \simeq 0.55 \mu\text{M}$  and  $[Cro_T] \simeq 0.0 \mu\text{M}$  values this becomes a nonlinear algebraic

equation of  $\Delta G_{RL}$  which, when solved with the aid of Octave's algorithm "fsolve" gives:

$$\Delta G_{RL} \simeq -3.1 \text{ kcal/mol.}$$

## APPENDIX B: DIMERIZATION KINETICS

Consider the following chemical reaction:



In this equation,  $a_2$  represents a dimer of chemical species  $a$ , and  $k_+$  and  $k_-$  are the forward and backward reaction rates, respectively.

In a state of chemical equilibrium the following relation is satisfied,

$$[a]^2 = K_D [a_2],$$

where  $K_D = k_-/k_+$  is the so-called dissociation constant and  $[x]$  represents the concentration of species  $x$ . Let  $[a_T]$  be the total monomer concentration:

$$[a_T] = [a] + 2[a_2].$$

The last two equations constitute a complete set of equations for the variables  $[a]$  and  $[a_2]$ . By solving for  $[a_2]$  we obtain the following expression for the dimer concentration in terms of  $a_T$  and  $K_D$ ,

$$[a_2] = \frac{[a_T]}{2} = \frac{K_D}{8} \left[ 1 + 8 \frac{[a_T]}{K_D} - 1 \right].$$

We wish to thank Olivier Landry and Miryam Elouneq-Jamroz for their collaboration in this project.

This work was supported by COFAA-IPN (México), EDI-IPN (México), CONACyT (México), MITACS (Canada), the Natural Sciences and Engineering Research Council (NSERC grant OGP-0036920, Canada), and Le Fonds pour la Formation de Chercheurs et l'Aide à la Recherche (FCAR grant 98ER1057, Québec).

## REFERENCES

- Ackers, G. K., A. D. Johnson, and M. A. Sea. 1982. Quantitative model for gene regulation by  $\lambda$  phage repressor. *Proc. Natl. Acad. Sci. USA*. 79:1129–1133.
- Arkin, A., J. Ross, and H. H. McAdams. 1998. Stochastic kinetic analysis of developmental pathway bifurcation in phage  $\lambda$ -infected *Escherichia coli* cells. *Genetics*. 149:1633–1648.
- Aurell, E., S. Brown, J. Johnson, and K. Sneppen. 2002. Stability puzzles in phage  $\lambda$ . *Phys. Rev.* E65:051914.
- Aurell, E., and K. Sneppen. 2002. Epigenetics as a first exit problem. *Phys. Rev. Lett.* 88:048101.
- Bremer, H., and P. P. Dennis. 1996. Modulation of chemical composition and other parameters of the cell by growth rate. In *Escherichia coli and Salmonella thyphimurium: Cellular and Molecular Biology*, Vol. 2. F. C. Neidhart, R. Curtis, J. L. Ingraham, E. C. C. Lin, K. B. Low, B. Magasanik, W. S. Reznikoff, M. Riley, M. Schaechter, and H. E. Umbarger, editors. American Society for Microbiology, Washington, DC. 1553–1569.
- Burz, D., D. Becket, N. Benson, and G. K. Ackers. 1994. Self-assembly of bacteriophage  $\lambda$  CI repressor: effects of single-site mutations on the monomer-dimer equilibrium. *Biochemistry*. 33:8399–8405.
- Court, D., B. Crombrughe, S. Adhya, and M. Gottesman. 1980. Bacteriophage lambda Hin function II. Enhanced stability of lambda messenger RNA. *J. Mol. Biol.* 138:731–743.

- Darling, P. J., J. M. Holt, and G. K. Ackers. 2000a. Couple energetics of  $\lambda$  *cro* repressor self-assembly and site-specific DNA operator binding. I: Analysis of *cro* dimerization from nanomolar to micromolar concentrations. *Biochemistry*. 39:11500–11507.
- Darling, P. J., J. M. Holt, and G. K. Ackers. 2000b. Coupled energetics of  $\lambda$  *cro* repressor self-assembly and site-specific DNA operator binding. II: Cooperative interactions of *cro* dimers. *J. Mol. Biol.* 302:625–638.
- Dodd, I. B., A. J. Perkins, D. Tsemitsidis, and B. Egan. 2001. Octamerization of  $\lambda$  CI repressor is needed for repression of  $P_{RM}$  and efficient switching from lysogeny. *Genes & Development*. 15:3013–3022.
- Draper, D. E. 1996. Translational initiation. In *Escherichia coli* and *Salmonella typhimurium*: Cellular and Molecular Biology, Vol. 1. F. C. Neidhart, R. Curtis, J. L. Ingraham, E. C. C. Lin, K. B. Low, B. Magasanik, W. S. Reznikoff, M. Riley, M. Schaechter, and H. E. Umbarger, editors. American Society for Microbiology, Washington, DC. 902–908.
- Fong, R. S., S. Woody, and G. N. Gussing. 1994. Direct and indirect effects of mutations in  $\lambda P_{RM}$  on open complex formation at the divergent  $P_R$  promoter. *J. Mol. Biol.* 240:119–120.
- Giladi, H., M. Gottesman, and A. B. Oppenheim. 1990. Integration host factor stimulates the phage lambda pL promoter. *J. Mol. Biol.* 213: 109–121.
- Gottesman, M. 1999. Bacteriophage  $\lambda$ : The untold story. *J. Mol. Biol.* 293:177–180.
- Hawley, D. K., A. D. Johnson, and W. R. McClure. 1985. Functional and physical characterization of transcription initiation complexes in the bacteriophage  $\lambda O_R$  region. *J. Biol. Chem.* 260:8618–8626.
- Hwang, J. J., S. Brown, and G. N. Gussin. 1988. Characterization of a doubly mutant derivative of the lambda  $P_{RM}$  promoter. Effects of mutations on activation of  $P_{RM}$ . *J. Mol. Biol.* 200:695–708.
- Kennell, D., and H. Riezman. 1977. Transcription and translation initiation frequencies of the *Escherichia coli lac* operon. *J. Mol. Biol.* 114:1–21.
- Leiv, L., and V. Kollin. 1967. Utilization and degradation of lactose operon mRNA in *Escherichia coli*. *J. Mol. Biol.* 24:247–259.
- Li, M., W. R. McClure, and M. Susskind. 1997. Changing the mechanism of transcriptional activation by phage  $\lambda$  repressor. *Proc. Natl. Acad. Sci. USA*. 94:3691–3696.
- Little, J. W., D. P. Shepley, and D. W. Wert. 1999. Robustness of a gene regulatory circuit. *EMBO J.* 18:4299–4307.
- McAdams, H. H., and L. Shapiro. 1995. Circuit simulation of genetic networks. *Science*. 269:650–656.
- Meyer, B. J., R. Maurer, and M. Ptashne. 1980. Gene regulation at the right operator ( $O_R$ ) of bacteriophage lambda. II.  $O_{R1}$ ,  $O_{R2}$ , and  $O_{R3}$ : Their roles in mediating the effects of repressor and *cro*. *J. Mol. Biol.* 139: 163–194.
- Pakula, A. A., V. B. Young, and R. T. Sauer. 1986. Bacteriophage lambda *cro* mutations: effects on activity and intracellular degradation. *Proc. Natl. Acad. Sci. USA*. 83:8829–8833.
- Ptashne, M. 1986. A Genetic Switch, Gene Control and Phage Lambda. Cell Press, Cambridge, MA.
- Ptashne, M., and A. Gann. 2000. Genes & Signals. Cold Spring Harbor Laboratory Press, New York.
- Reintz, J., and J. R. Vaisnys. 1990. Theoretical and experimental analysis of the phage lambda genetic switch implies missing levels of cooperativity. *J. Theor. Biol.* 145:295–318.
- Rozanov, D. V., R. D'Ari, and S. P. Sineoky. 1998. RecA-independent pathways of lambdaoid prophage induction in *Escherichia coli*. *J. Bacteriol.* 180:6306–6315.
- Shea, M. A., and G. K. Ackers. 1985. The  $O_R$  control system of bacteriophage lambda, a physical-chemical model for gene regulation. *J. Mol. Biol.* 181:211–230.